

One Perturbation is Enough: On Generating Universal Adversarial Perturbations against Vision-Language Pre-training Models

Hao Fang* Jiawei Kong* Wenbo Yu Bin Chen[†] Jiawei Li

Hao Wu Shu-Tao Xia Ke Xu

Tsinghua Shenzhen International Graduate School, Tsinghua University
Harbin Institute of Technology, Shenzhen

fang-h23@mails.tsinghua.edu.cn

Abstract

Vision-Language Pre-training (VLP) models have exhibited unprecedented capability in many applications by taking full advantage of the learned multimodal alignment. However, previous studies have shown they are vulnerable to maliciously crafted adversarial samples. Despite recent success, these attacks are generally instance-specific and require generating perturbations for each input sample. In this paper, we reveal that VLP models are also susceptible to the instance-agnostic universal adversarial perturbation (UAP). Specifically, we design a novel Contrastive-training Perturbation Generator with Cross-modal conditions (C-PGC). In light that the pivotal multimodal alignment in VLP models is achieved via contrastive learning, we devise to turn this powerful weapon against VLP models themselves. I.e., we employ a malicious version of contrastive learning to train the proposed generator using our carefully crafted positive and negative image-text pairs. Once training is complete, the generator is able to produce universal perturbations that can essentially destroy the established alignment relationship in VLP models. Besides, C-PGC fully utilizes the characteristics of Vision-and-Language (V+L) scenarios by incorporating both unimodal and cross-modal information as effective guidance. Extensive experiments show that C-PGC successfully forces adversarial samples to move away from their original area in the VLP model’s feature space, thus fundamentally enhancing attack performance across various victim models and V+L tasks.

1. Introduction

Vision-Language Pre-training (VLP) models have recently demonstrated remarkable efficacy in a wide range of Vision-and-Language (V+L) tasks. By self-supervised pre-training

*Equal contribution

[†]Corresponding Author

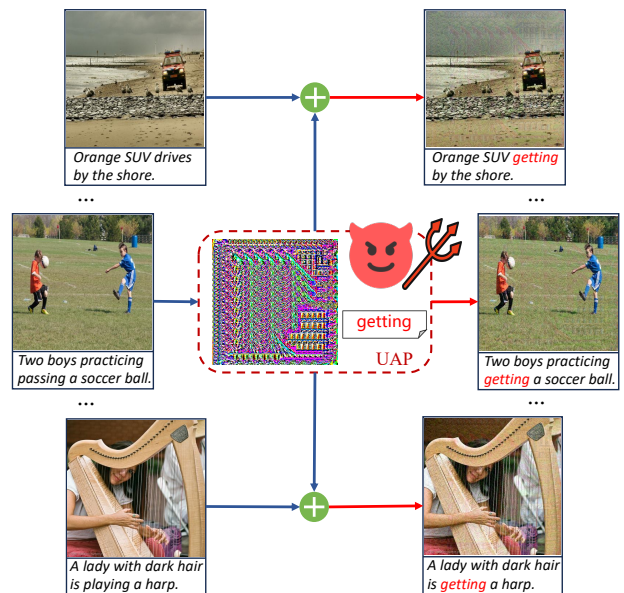


Fig. 1: Illustration of universal adversarial attacks. With only a pair of image-text perturbations, the proposed method can effectively mislead different VLP models on diverse V+L tasks.

on large-scale image-text pairs, VLP models efficiently align cross-modal features and capture rich information from the aligned multimodal embeddings, thereby providing expressive representations for various applications.

Adversarial attacks [7], which aim to deceive models during inference time, have attracted extensive attention due to their significant threat to security-critical scenarios [15]. Recent studies have shown that VLP models are also vulnerable to adversarial samples. The pioneering work Co-Attack [48] proposes the first multimodal attack that simultaneously perturbs both image and text modalities and displays excellent performance. However, Co-Attack only considers relatively easier white-box attacks where victim models are completely accessible. To handle more practical black-box settings, subsequent studies propose various

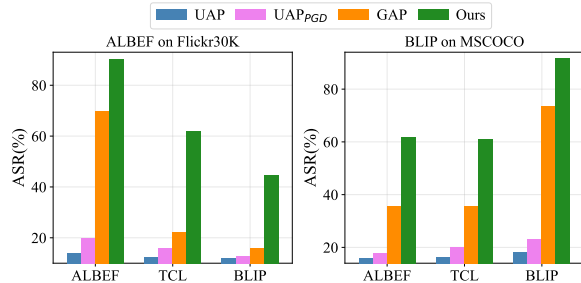


Fig. 2: Performance of existing UAP on text retrieval with ALBEF [23] and BLIP [24] as surrogate models. Note that UAP [31] is initially based on DeepFool [30] and the corresponding PGD-learned version UAP_{PGD} is provided for a fair comparison.

transferable adversarial samples generated on an available surrogate model to fool other inaccessible models. Specifically, SGA [29] significantly improves the adversarial transferability through the set-level cross-modal guidance obtained from data augmentations. Subsequently, TMM [41] proposes to jointly destroy the modality-consistency features within the clean image-text pairs and include more modality-discrepancy features in the perturbations to further enhance transferability. While existing methods have achieved great success, they are all instance-specific and need to generate a perturbation for each input pair, which results in substantial computational overhead. Meanwhile, universal adversarial attacks (illustrated in Fig. 1), as an efficient instance-agnostic approach that uses only one Universal Adversarial Perturbation (UAP) to conduct attacks, have not been fully investigated for VLP models. This naturally leads to a question, *is it possible to design a UAP that can deceive VLP models across different image-text pairs?*

Motivation. To this end, we make an intuitive attempt to transplant renowned approaches UAP [31] and GAP [37] to attack several VLP models by maximizing the distance between the embeddings of the adversarial image and its matched texts. Unfortunately, Fig. 2 demonstrates that these methods yield unsatisfactory attack success rates (ASR), especially for black-box attacks. Empirically, this failure stems from their narrow focus on the image modal, disregarding the other modality and the multimodal information that plays a pivotal role in VLP models. To overcome this challenge, we revisit VLP models’ basic training paradigm and emphasize that regardless of the downstream V+L tasks, their achieved outstanding performance is heavily reliant on the well-established multimodal alignment, which draws the embeddings of matched image-text pairs closer while distancing those of non-matched pairs. In light of this consideration, we argue that the core of an effective universal adversarial attack is to obtain a UAP that can fundamentally destroy this learned alignment relationship to mislead VLP models into making incorrect decisions. Besides, Fig. 2 shows that the generator-based GAP consis-

tently outperforms UAP methods, due to the excellent distributional modeling capability of generators. This suggests the superiority of the generative paradigm, which is also corroborated by numerous studies [16, 17].

Based on these insights, we propose a novel generative framework that learns a Contrastive-training Perturbation Generator with Cross-modal conditions (C-PGC) to launch universal attacks on VLP models. To essentially destroy the multimodal alignment, we devise to utilize VLP models’ most powerful weapons to attack against themselves. *I.e.*, utilize the contrastive learning mechanism to train the generator based on maliciously constructed image-text pairs that completely violate the correct V+L matching relationship, to produce perturbation that pushes the embeddings of matched pairs apart while pulling those of non-matched ones together. Moreover, most previous studies [29, 48, 49] simply exploit the crucial cross-modal information by maximizing the feature distance between samples of different modalities to optimize perturbations, without deeper exploration for attack enhancement. In contrast, we fully harness V+L characteristics by refining the generator architecture to incorporate cross-modal knowledge through cross-attention mechanisms for better guidance. Besides, we also consider the intra-modal influence and introduce a unimodal distance loss to further improve attack effectiveness. We highlight that the proposed framework is seamlessly compatible with text perturbation generation, achieving a truly multimodal universal attack that benefits from the synergy between V+L modalities. Our contributions are as follows:

- We propose C-PGC, a novel perturbation generator conditioned on cross-modal knowledge, to produce both image and text UAPs for powerful attacks on VLP models.
- We design a malicious contrastive learning paradigm that incorporates both unimodal and multimodal guidance to train the generator to produce UAP that can essentially disrupt the multimodal alignment in VLP models.
- Extensive experiments on 6 various VLP models across diverse V+L tasks reveal that our method achieves outstanding attack performance in different scenarios.

2. Related Work

2.1. Vision-Language Pre-training Models

VLP models are pre-trained on massive image-text pairs to learn the semantic correlations across modalities and serve diverse multimodal user demands [8, 13]. We next illustrate the basis of VLP models from multiple perspectives.

Architectures. Based on the ways of multimodal fusion, the architectures of VLP models can be classified into two types: *single-stream* and *dual-stream* architectures. Single-stream architectures [9, 25] directly concatenate the text and image features, and calculate the attention in the same Transformer block for multimodal fusion.

On the contrary, dual-stream architectures [24, 38] separately feed the text and image features to different Transformer blocks and leverage the cross-attention mechanism for multimodal fusion. Generally, single-stream architectures are more parameter-efficient than dual-stream architectures since they adopt the same set of parameters in a Transformer block for the text and image modalities.

Pre-training Objectives. The pre-training objectives for VLP models mainly include *masked feature completion*, *multimodal feature matching*, and *specific downstream objectives*. Masked feature completion [9] encourages VLP models to predict the deliberately masked tokens based on the remaining unmasked tokens. Multimodal feature matching [23] pre-trains VLP models to precisely predict whether the given image-text pairs are matched. Specific downstream objectives [2] directly utilize the training objectives of downstream tasks (*e.g.*, visual question answering) for pre-training VLP models.

Downstream Tasks. In this paper, we mainly consider the following multimodal downstream tasks: (1) Image-text retrieval (ITR) [42]: finding the most matched image for the given text and vice versa, including image-to-text retrieval (TR) and text-to-image retrieval (IR). (2) Image caption (IC) [4]: generating the most suitable descriptions for the given image. (3) Visual grounding (VG) [20]: locating specific regions in the image that correspond with the given textual descriptions. (4) Visual entailment (VE) [43]: analyzing the input image and text and predicting whether their relationship is entailment, neutral, or contradiction.

2.2. Adversarial Attacks

Instance-specific Attacks on VLP Models. The adversarial robustness of VLP Models has already become a research focus. Early works [22, 45] impose perturbations only on single modality and lack cross-modal interactions when attacking multimodal models. To address this issue, Co-Attack [48] conducts the first multimodal white-box attacks on VLP models. On the basis of Co-Attack, [29] extends the attacks to more rigorous black-box settings and proposes SGA, which utilizes set-level alignment-preserving argumentations with carefully designed cross-modal guidance. However, [41] points out that SGA fails to fully exploit modality correlation, and proposes TMM to better leverage cross-modal interactions by tailoring both the modality-consistency and modality-discrepancy features. Nonetheless, these methods are all instance-specific and need to craft perturbations for each input pair.

Universal Adversarial Examples. Universal adversarial attacks [31, 32, 51] aim to deceive the victim model by exerting a uniform adversarial perturbation to all samples. These attacks save the redundant procedures of redesigning perturbations for each input sample and are hence more efficient than instance-specific methods. Generally, univer-

sal adversarial attacks can be categorized into optimization-based [28, 31, 40] and generation-based [3, 17, 18, 51] methods. Benefiting from the powerful modeling abilities of generative models, generation-based methods are more versatile and can produce more natural samples than optimization-based ones. A concurrent work ETU [49] also investigates UAP on VLP models and proposes a data augmentation named ScMix. However, *ETU adopts a non-generative approach that narrowly focuses on image UAP, failing to constitute a truly multimodal attack for VLP models*. Moreover, ETU demonstrates insufficient attack effects, especially for black-box transferability. In contrast, we propose a generative multimodal attack framework based on a malicious variant of contrastive learning, which yields UAP with strong attack effects and high transferability.

3. Universal Multimodal Attacks

In this section, we first present the problem statement of universal adversarial attacks on VLP models. Next, we introduce the overview of our framework. Finally, we illustrate the detailed design of the proposed C-PGC.

3.1. Problem Statement

We define an input image-text pair as (v, t) and denote e_v and e_t as the image and text embeddings encoded by the image encoder $f_I(\cdot)$ and text encoder $f_T(\cdot)$ of the targeted VLP model $f(\cdot)$. Let \mathcal{D}_s be an available dataset consisting of image-text pairs collected by a malicious adversary. The attack objective is to utilize \mathcal{D}_s to train a generator $G_w(\cdot)$ for producing a powerful pair of universal image-text perturbations (δ_v, δ_t) that can affect the vast majority of test dataset \mathcal{D}_t to fool models into making incorrect decisions. Formally, the attack goal can be formulated as:

$$\mathcal{T}(f(v + \delta_v, t \oplus \delta_t)) \neq y, \text{ s.t. } \|\delta_v\|_\infty \leq \epsilon_v, \|\delta_t\|_0 \leq \epsilon_t, \quad (1)$$

where $\mathcal{T}(\cdot)$ denotes the operation that uses the output V+L features to obtain the final predictions, \oplus indicates the text perturbation strategy [29, 48] that replaces certain important tokens of the original sentence with crafted adversarial words, and y is the correct prediction of the considered V+L task. To ensure the perturbation’s imperceptibility, we constrain the pixel-level image perturbation with l_∞ norm of a given budget ϵ_v . Following previous studies [29, 41, 48], the textual perturbation is token-level and the stealthiness is accordingly constrained by the number of modified words ϵ_t . To ensure the stealthiness of text perturbation, we apply a rigorous restriction that permits only a single word to be substituted ($\epsilon_t = 1$). On the premise of imperceptibility, the attacker attempts to generalize the crafted UAP to a wider range of test data and victim models.

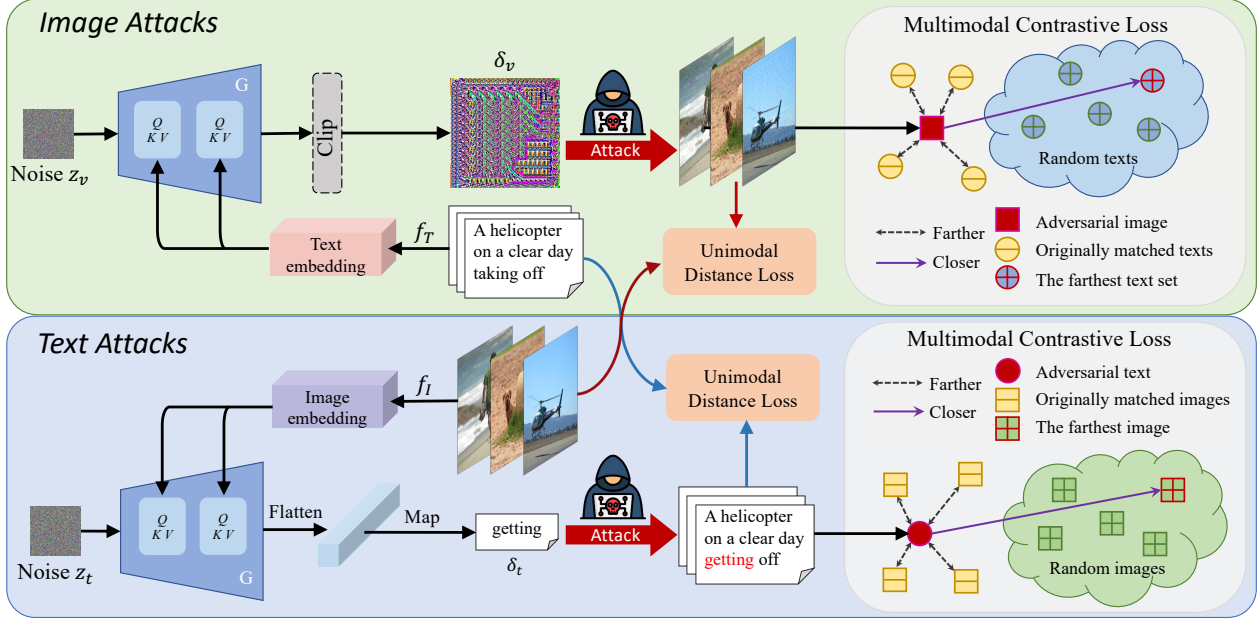


Fig. 3: An overview of our proposed universal adversarial attack. Benefiting from the well-designed unimodal distance loss \mathcal{L}_{Dis} and multimodal contrastive loss \mathcal{L}_{CL} , the generator $G_w(\cdot)$, conditioned with cross-modal embeddings, learns rich knowledge from features of different modalities and thus produces δ_v and δ_t of superior generalization ability across diverse models and downstream tasks.

3.2. Overview of the Proposed Framework

The overview of C-PGC is depicted in Fig. 3. We adopt a multimodal perturbation strategy and generate perturbations for both image and text modalities. Given the high similarity between the workflows of image and text, we then take image attacks as an example for illustration.

Firstly, a fixed noise z_v is randomly initialized and subsequently fed into the conditional generator. For each image v and its descriptions \mathbf{t} , the generator $G_w(\cdot)$ translates the input noise z_v into the adversarial perturbation δ_v that is of the same size as v . During generation, the network G_w additionally benefits from cross-modal information by integrating the embedding of text descriptions corresponding to the current input image v , *i.e.*, $\delta_v = G_w(z_v; f_T(\mathbf{t}))$. Next, the generated adversarial noise δ_v is injected into the clean image to obtain the adversarial image via $v_{adv} = v + \delta_v$. To better guide the training process, we design two effective unimodal and multimodal losses as our optimization objectives. Unimodal loss is straightforward and aims to push the adversarial images away from the clean images in the latent embedding space, while multimodal loss is based on contrastive learning using our manually constructed positive and negative samples to strongly destroy the image-text matching relationship achieved by feature alignment. Once we finish training C-PGC using the proposed loss function, the input fixed noise is transformed into a UAP with great generalization and transferability.

3.3. Detailed Design of C-PGC

Next, we provide a detailed introduction to each of the proposed designs. Note that we primarily discuss the image attack as an example, given that the design of the text attack is completely symmetrical. The pseudocode of the training procedure is provided in Appendix A.

Perturbation Generator Conditioned on Cross-modal knowledge. Previous generative universal attacks [3, 17] have shown excellent efficacy in fooling the discriminative models. Nevertheless, since existing generative attacks are limited to a single modality, directly utilizing the off-the-shelf generators might fail to leverage the multimodal interactions in these special V+L scenarios. To address this limitation, we additionally introduce cross-modal embeddings as auxiliary information to further facilitate the process of perturbation generation. Specifically, we modify the architecture of existing decoder-based generators by adding several cross-attention modules that have been proven effective in tasks with multiple input modalities. The obtained textual embeddings e_t encoded by $f_T(\cdot)$ are then incorporated into our generator through:

$$Q = \mathbf{h}_t W_q, K = e_t W_k, V = e_t W_v, \\ \text{Attention}(Q, K, V) = \text{softmax} \left(\frac{QK^T}{\sqrt{d}} \right) \cdot V, \quad (2)$$

where $\mathbf{h}_t \in \mathbb{R}^{B \times d_\alpha}$ is the flattened intermediate features within $G_w(\cdot)$, and $W_q \in \mathbb{R}^{d_\alpha \times d}$, $W_k \in \mathbb{R}^{512 \times d}$, $W_v \in \mathbb{R}^{512 \times d}$ are the optimized parameters of attention modules.

Multimodal Contrastive Loss. The preceding analysis regarding the failures of existing UAP attacks encourages us to design a loss function that can guide the generated UAP to break the learned multimodal feature alignment. Motivated by the fact that contrastive learning underpins the cross-modal alignment, we advocate leveraging this mechanism to attack VLP models themselves by contrastively training our C-PGC to essentially disrupt the benign alignment relationship. Concretely, we adopt the widely recognized InfoNCE [19] as our basic contrastive loss.

To establish the contrastive paradigm, we first define the adversarial image v_{adv} as the anchor sample. Besides, it is also necessary to construct an appropriate set of positive and negative samples. Based on the fundamental objective of our attack, it is natural to leverage the originally matched text description set $\mathbf{t} = \{t_1, t_2, \dots, t_M\}$ as negative samples \mathbf{t}_{neg} to amplify the discrepancy between matched image-text pairs in the feature space of VLP models. Additionally, we need to select a set of positive samples to further pull the adversarial image v_{adv} away from its corresponding text descriptions \mathbf{t} . To this end, we propose a *farthest selection strategy*, which associates the anchor image v_{adv} with target texts \mathbf{t}_{pos} whose embeddings differ significantly from that of the original clean image v , to reach a more strong disruption of the multimodal alignment. Specifically, we randomly sample a batch of text sets from \mathcal{D}_s and select the text set with the largest feature distances from the current image v as positive samples, *i.e.*, $\mathbf{t}_{pos} = \{t'_1, t'_2, \dots, t'_K\}$. Moreover, we utilize data augmentations that resize the clean v into diverse scales and apply random Gaussian noise to acquire a more diverse image set $\mathbf{v} = \{v_1, v_2, \dots, v_N\}$ for set-level guidance [29]. With these well-constructed positive and negative samples, the multimodal contrastive loss \mathcal{L}_{CL} can be formulated as:

$$\mathcal{L}_{CL} = \log \frac{\sum_{i=1}^N \sum_{j=1}^M s(v_i + \delta_v, t_j)}{\sum_{i=1}^N \sum_{j=1}^M s(v_i + \delta_v, t_j) + \sum_{i=1}^N \sum_{j=1}^K s(v_i + \delta_v, t'_j)}, \quad (3)$$

where δ_v is the universal image perturbation; $s(v, t) = \exp(\text{sim}(f_I(v), f_T(t))/\tau)$, where τ denotes the temperature parameter and $\text{sim}(\cdot, \cdot)$ represents the cosine similarity.

Unimodal Distance Loss. Apart from the multimodal guidance, we also consider the unimodal influence by directly pushing adversarial images away from their initial visual semantic area to improve the attack. Similarly, the input image v also undergoes resizing and noise perturbation to generate the augmented image set $\mathbf{v} = \{v_1, v_2, \dots, v_N\}$ for set-level guidance. Then, we craft the adversarial image through $v_{adv} = v + \delta_v$ and process v_{adv} with the same augmentation operation to obtain the adversarial image set $\mathbf{v}_{adv} = \{v_1^{adv}, v_2^{adv}, \dots, v_N^{adv}\}$. Finally, we minimize the

negative Euclidean distance between the embeddings of adversarial images and clean images to optimize the UAP generator. Formally, the loss \mathcal{L}_{Dis} is formulated as:

$$\mathcal{L}_{Dis} = - \sum_{i=1}^N \sum_{j=1}^N \|f_I(v_i^{adv}) - f_I(v_j)\|_2. \quad (4)$$

Taking advantage of the unimodal guidance, \mathcal{L}_{Dis} ensures an effective optimization direction during the generator training and further enhances the attack effectiveness.

Training Objective. With the above two well-designed loss terms \mathcal{L}_{Dis} and \mathcal{L}_{CL} , the overall optimization objective of our conditional generator for image attacks can be formulated as:

$$\begin{aligned} \min_w \mathbb{E}_{(v, \mathbf{t}) \sim \mathcal{D}_s, \mathbf{t}_{pos} \sim \mathcal{D}_s} (\mathcal{L}_{CL} + \lambda \mathcal{L}_{Dis}), \\ \text{s.t. } \|G_w(z_v; f_T(\mathbf{t}))\|_\infty \leq \epsilon_v, \end{aligned} \quad (5)$$

where λ is the pre-defined hyperparameter to balance the contributions of \mathcal{L}_{CL} and \mathcal{L}_{Dis} . By training the network with the proposed loss function over the entire data distribution of the multimodal training dataset \mathcal{D}_s , the generator $G_w(\cdot)$ is optimized to generate UAPs that push the features of mismatched image-text pairs together while pulling the embeddings of the matched ones apart. This finally enables the generation of UAPs with strong generalization capabilities and high adversarial transferability.

Text Modality Attacks. In textual attacks, the generator architecture and training loss are completely symmetrical with those of image attacks. Correspondingly, embeddings of the matched image v are used as the cross-modal conditions for the generator. Given an adversarial text t_{adv} as the anchor sample, we use the set $\mathbf{v} = \{v_1, v_2, \dots, v_N\}$ scaled from the originally matched image v as negative samples while the $\mathbf{v}' = \{v'_1, v'_2, \dots, v'_N\}$ augmented from the farthest image v' within the randomly sampled image set as positive samples to formulate the \mathcal{L}_{CL} loss. \mathcal{L}_{Dis} is consequently calculated as the negative Euclidean distance between the embeddings of t_{adv} and the clean input t . Accordingly, the conditional generator is utilized to output the adversarial textual embeddings, which are subsequently mapped back to the vocabulary space to obtain a universally applicable word-level perturbation.

A notable distinction between image and text attacks is the way to inject adversarial perturbations. We align with previous studies [29, 41, 48] and apply the token-wise substitute strategy that replaces certain important words in the original sentence with crafted adversarial words. Prior to the word replacement, a meticulous process is undertaken to identify the most optimal position within the sentence to insert the perturbation. Our strategy intends to replace the words that are more likely to have a greater influence during decision-making. Concretely, for each word w_i within

a given sentence, we compute the distance between the embeddings of the original sentence and the w_i -masked version to determine its contribution. By convention, the imperceptibility of text UAP is controlled by the number of modified words ϵ_t [6]. As aforementioned, we set $\epsilon_t = 1$ for high stealthiness, *i.e.*, choose the single word exerting the highest feature distance as the target for replacement.

4. Experiments

To comprehensively validate the effectiveness of C-PGC, we conduct experiments on diverse downstream V+L tasks across multiple VLP models. Please see more experiments including **performance under defenses, cross-domain attacks, loss analysis, and visualization** in the Appendix.

4.1. Experimental Setup

Downstream tasks and datasets. We conduct a comprehensive study of C-PGC on four downstream V+L tasks, including image-text retrieval (ITR), image captioning (IC), visual grounding (VG), and visual entailment (VE). For ITR tasks, we employ the Flickr30K [36] and MSCOCO [27] datasets which are commonly used in previous works [29, 48]. The MSCOCO is also adopted for evaluating the IC task. For VG and VE tasks, we evaluate on SNLI-VE [43] and RefCOCO+ [46] datasets respectively.

Models. We conduct experiments on a wide range of VLP models including ALBEF [23], TCL [44], X-VLM [47], CLIP_{VIT} [38], CLIP_{CNN} [38], and BLIP [24]. Note that for different V+L tasks, we correspondingly select different VLP models for evaluation based on their capability [41]. For instance, among the six considered VLP models, only ALBEF, TCL, and X-VLM can handle VG tasks, while only ALBEF and TCL can deal with VE tasks.

Baselines. We transplant the representative GAP [37] to V+L scenarios by appropriately editing its original loss function [29]. We also consider a concurrent UAP study ETU [49], which adopts a non-generative method that narrowly focuses on image perturbation, despite the multimodal nature of V+L scenarios. Note that it implements several versions and we report their best results.

Implementation details. Following the SGA [29], we adopt Karpathy split [21] to preprocess the dataset and build the test set for evaluation. The test set is disjoint with the generator’s training data for rigorous assessment. To ensure perturbation invisibility, we follow [41] and limit the perturbation budgets ϵ_v to 12/255 and ϵ_t to 1. For augmentation, we resize the original images into five scales $\{0.5, 0.75, 1, 1.25, 1.5\}$, and apply Gaussian noise $\mathcal{N}(0, 0.5^2)$. See Appendix B for more details.

4.2. Universal Attack Effectiveness

To align with previous studies [29, 48], we first consider the typical V+L task image-text retrieval and calculate the ASR

as the proportion of successful adversarial samples within the originally correctly predicted pairs. We present the performance based on R@1 retrieval results in Table 1. Appendix C supplements the results of R@5 and R@10.

White-box attack performance. By observing the white-box ASR in the gray-shaded area, we demonstrate that the proposed algorithm stably achieves excellent ASR on all the evaluated VLP models, validating the outstanding capability of the produced UAP. With only a single pair of perturbations, we reach a noteworthy average white-box ASR of nearly 90% on two large datasets in terms of both TR and IR tasks. Compared with GAP [37] and ETU [49], the proposed method consistently enhances the fooling rates in the white-box scenario, confirming the great validity of our suggested multimodal contrastive-learning mechanism. Essentially, the exceptional performance stems from the efficacy of our generated UAP in destroying the alignment between the image and text modalities, thereby misleading the VLP model during inference.

Black-box attack performance. We also conduct thorough experiments regarding the adversarial transferability of the generated UAP by transferring from surrogate models to other inaccessible models. As demonstrated in Table 1, the proposed C-PGC displays great attack effects in the more realistic black-box scenarios, *e.g.*, 72.51% from ALBEF to CLIP_{CNN} for IR tasks. We highlight that the advantage of C-PGC over the concurrent study ETU is greatly amplified in the more challenging black-box scenarios, which achieves a significant average improvement of 17.76% on the Flickr30K dataset. These experimental results indicate that our generative contrastive learning framework does not overly rely on the encoded feature space tailored to the surrogate model. Conversely, it is well capable of transferring to breaking the multimodal alignment of other unseen target models, thus attaining superior adversarial transferability.

4.3. Evaluation on More Downstream Tasks

We then provide results on more downstream V+L tasks. Specifically, we consider Image Captioning (IC), Visual Grounding (VG), and Visual Entailment (VE). The results of VE are shown in Appendix C due to space limit.

Visual grounding. This is another common V+L task, which aims to locate the correct position in an image based on a given textual description. We conduct experiments on RefCOCO+ using ALBEF, TCL, and X-VLM as source and target models. Table 2 indicates that C-PGC brings a notable negative impact on the localization accuracy in both white-box and black-box settings, again verifying that the produced UAP strongly breaks the cross-modal alignment.

Image captioning. The objective of IC is to generate text descriptions relevant to the semantic content based on the given image. We use ALBEF, TCL, and BLIP as source models and attack the commonly used captioning model

Table 1. ASR (%) of different methods for image-text retrieval tasks on Flickr30k dataset. TR indicates text retrieval based on the input image, while IR is image retrieval using the input text. The results on the MSCOCO dataset are in Appendix C due to space limit.

Source	Method	ALBEF		TCL		X-VLM		CLIP _{VIT}		CLIP _{CNN}		BLIP	
		TR	IR	TR	IR	TR	IR	TR	IR	TR	IR	TR	IR
ALBEF	GAP	69.78	81.59	22.15	29.97	6.61	18.37	23.40	37.54	29.92	44.29	16.09	28.12
	ETU	78.01	84.56	29.92	35.91	14.33	22.03	23.77	39.20	33.55	47.69	22.61	32.28
	Ours	90.13	88.82	62.11	64.48	20.53	39.38	43.10	65.93	54.40	72.51	44.79	56.36
TCL	GAP	33.50	40.61	82.41	80.67	6.61	17.79	21.55	38.56	30.57	45.48	21.45	31.82
	ETU	28.26	35.03	90.48	87.57	9.65	20.56	25.00	39.68	36.14	49.33	18.93	29.19
	Ours	50.26	56.29	94.93	90.64	14.94	33.96	46.92	66.41	52.98	70.66	35.75	52.52
X-VLM	GAP	16.14	24.43	17.08	26.20	90.24	85.98	24.51	41.15	42.62	53.08	16.19	25.74
	ETU	12.33	21.93	13.98	24.04	93.19	90.85	23.89	39.62	35.62	51.19	12.09	23.59
	Ours	24.46	47.77	29.19	50.15	93.29	91.90	43.47	66.03	59.20	72.79	32.39	52.24
CLIP _{VIT}	GAP	11.72	23.34	15.32	26.39	8.54	20.48	85.73	90.45	48.83	60.78	14.83	26.46
	ETU	14.80	25.23	21.22	30.87	10.87	24.96	84.14	90.45	57.51	65.51	16.40	27.22
	Ours	23.23	38.67	25.05	41.79	15.85	35.59	88.92	93.05	66.06	75.42	26.71	45.70
CLIP _{CNN}	GAP	13.57	25.21	19.05	28.87	11.59	23.13	27.46	43.16	73.18	81.60	15.25	27.94
	ETU	8.94	20.59	13.25	24.41	8.94	20.82	21.92	40.51	91.71	92.40	11.15	23.82
	Ours	19.01	41.86	22.98	47.02	19.61	43.26	40.89	65.77	96.50	94.22	24.19	48.17
BLIP	GAP	12.23	23.94	14.49	25.44	6.91	17.81	20.32	37.00	26.81	43.59	47.21	73.33
	ETU	19.32	27.91	19.98	29.15	11.99	20.91	24.38	39.84	31.61	46.22	59.52	77.82
	Ours	32.17	44.40	33.44	44.51	18.60	35.53	43.35	60.26	48.96	66.95	71.82	82.82

Table 2. Performance of C-PGC on the visual grounding task. The first row displays the source models, and the Baseline indicates the clean performance of the target model on clean data.

Target	Baseline			ALBEF			TCL			X-VLM		
	Val	TestA	TestB	Val	TestA	TestB	Val	TestA	TestB	Val	TestA	TestB
ALBEF	58.4	65.9	46.2	37.1	39.8	32.0	42.2	46.9	35.2	37.6	40.2	33.0
TCL	59.6	66.8	48.1	43.6	47.8	36.9	39.0	41.4	33.6	39.5	41.7	34.1
X-VLM	70.8	67.8	61.8	51.8	54.7	47.7	52.7	55.9	47.8	33.1	34.7	28.8

Table 3. Performance of C-PGC on image captioning task. The Baseline represents the clean performance. The surrogate is BLIP.

Source	B@4	METEOR	ROUGE.L	CIDEr	SPICE
Baseline	39.7	31.0	60.0	133.3	23.8
ALBEF	30.1	23.7	51.2	92.5	17.5
TCL	29.5	23.5	51.0	88.9	17.3
BLIP	21.2	19.1	45.5	62.5	13.7

BLIP. Similar to SGA [29], several typical evaluation metrics of IC are calculated to measure the quality of generated captions, including BLEU [35], METEOR [5], ROUGE [26], CIDEr [39], and SPICE [1]. The results in Table 3 demonstrate that our algorithm again displays prominent attack effectiveness, *e.g.*, the crated UAP induces notable drops of 10.2% and 9% in the B@4 and ROUGE.L respectively when transferred from TCL to BLIP.

4.4. Ablation Study

This part employs ALBEF [23] as the surrogate model and provides ablation studies on Flickr30K. We begin our analysis on the contribution of each proposed technique. Next, we examine the sensitivity of certain hyperparameters.

The effect of \mathcal{L}_{CL} and \mathcal{L}_{Dis} . To investigate the impact of the proposed loss terms, we introduce two variants C-PGC_{CL} and C-PGC_{Dis} that remove \mathcal{L}_{CL} and \mathcal{L}_{Dis} from the overall training loss respectively. As shown in Table 4, the removal of \mathcal{L}_{CL} leads to significant degradation, particularly for black-box transferable attacks. *E.g.*, a 27.12% ASR drop occurs in TR tasks when transferring from ALBEF to TCL. This validates the considerable contribution of \mathcal{L}_{CL} to guarantee a successful attack. Regarding the influence of \mathcal{L}_{Dis} , we demonstrate that the unimodal guidance further enhances the attack on the basis of \mathcal{L}_{CL} . Especially in white-box scenarios, \mathcal{L}_{Dis} brings a 10.59% increase in

Table 4. ASR (%) of C-PGC and its variants averaged across six target models on retrieval tasks.

Method	ALBEF		TCL		X-VLM		CLIP _{VIT}		CLIP _{CNN}		BLIP	
	TR	IR	TR	IR	TR	IR	TR	IR	TR	IR	TR	IR
C-PGC	90.13	88.82	62.11	64.48	20.53	39.38	43.10	65.93	54.40	72.51	44.79	56.36
C-PGC _{CL}	76.46	77.58	34.99	47.55	14.33	33.61	42.98	62.81	46.11	65.58	27.13	46.44
C-PGC _{Dis}	79.54	82.46	56.52	62.21	20.24	38.26	39.78	65.10	52.20	71.01	42.43	55.52
C-PGC _{Rand}	61.87	65.17	43.69	52.54	19.51	35.47	40.33	65.77	54.15	70.62	39.43	52.59
C-PGC _{CA}	85.18	83.07	45.76	53.73	15.24	34.02	39.29	60.61	47.15	40.64	32.39	48.29

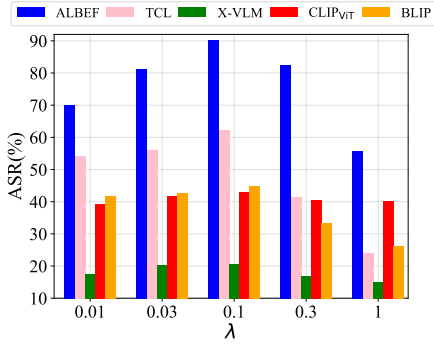


Fig. 4: ASR of five target models on TR tasks under various values of λ .

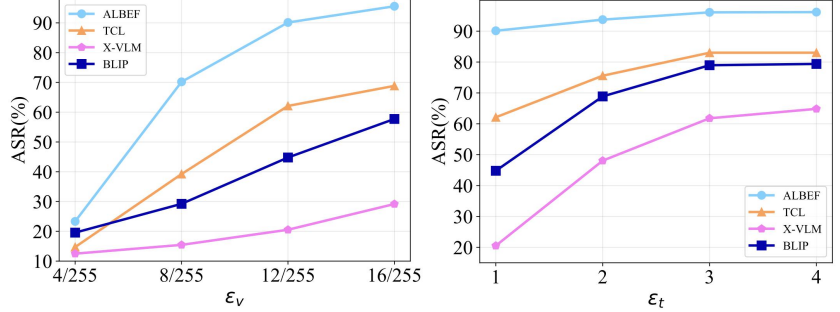


Fig. 5: ASR of five target models on the TR task under different values of perturbation budgets for ϵ_v and ϵ_t respectively.

the ASR of TR tasks on ALBEF. The proposed two loss terms complement each other and jointly underpin the generalizability and transferability of the produced UAP.

The effect of positive sample selection. To validate the *farthest selection strategy* for positive sample construction, we design another variant C-PGC_{Rand} that adopts randomly sampled data points as positive samples. Results in Table 4 reveal the necessity of the proposed selection strategy as it brings an average improvement of 25.96% in white-box ASR and 4.95% in black-box ASR. Moreover, we also find that if the positive samples are not adequately defined, adding the \mathcal{L}_{CL} would even harm the white-box performance (see C-PGC_{CL} and C-PGC_{Rand}). This highlights the significance of the proposed selection strategy.

The effect of cross-modal conditions. As aforementioned, cross-attention (CA) modules are introduced into the generator to exploit cross-modal information. We then design C-PGC_{CA} that cancels these CA layers to explore the influence. As expected, it causes a notable 9.78% average decrease across six target models, verifying its vital role in boosting attacks. Another finding is that C-PGC_{CA} induces a more pronounced drop in black-box attacks than white-box ones, indicating that cross-modal conditions exert a greater contribution to adversarial transferability.

Different regulatory factor λ . The value of λ is a critical factor as it adjusts the scales of the two loss terms \mathcal{L}_{CL} and \mathcal{L}_{Dis} . We evaluate the attack performance under various

values of λ to confirm the optimal value. Fig. 4 indicates that $\lambda = 0.1$ achieves superior performance.

Different perturbation budgets ϵ_v and ϵ_t . As shown in Fig. 5, we analyze varying perturbation budgets for ϵ_v and ϵ_t . Generally, the ASR increases with the larger perturbation magnitudes. Note that when $\epsilon_v = 4/255$, C-PGC’s performance is severely compromised since the budget 4/255 is too small to allow the UAP to carry enough information required to generalize to diverse data samples.

It also indicates that the improvement slows down as ϵ_v increases from 12/255 to 16/255. Thus, we select the moderate value of 12/255 to reach a balance between attack utility and imperceptibility. For text perturbation, ϵ_t exhibits a more profound influence on the black-box attacks. In our experiments, we strictly set $\epsilon_t = 1$ for invisibility. Attackers can adjust the value of ϵ_t in accordance with their demands to trade off the attack efficacy and perturbation stealthiness.

5. Conclusion

In this paper, we investigate the challenging task of universal adversarial attacks on VLP models. We begin by revealing the deficiency of existing UAP methods and empirically explaining the underlying reasons. Based on the analysis, we propose to break the crucial multimodal alignment in VLP models by designing a contrastive-learning generative UAP framework that leverages both unimodal and multimodal information to enhance the attack. Extensive experiments validate

the efficacy of C-PGC on diverse VLP models and V+L tasks. We highlight that the proposed method makes a significant step in exploring classic universal attacks in multimodal attacks and deepens our understanding of the mechanism underlying VLP models. We hope our work can promote future research on more sophisticated defenses to further strengthen the robustness of VLP models.

References

- [1] Peter Anderson, Basura Fernando, Mark Johnson, and Stephen Gould. Spice: Semantic propositional image caption evaluation. In *Computer Vision—ECCV 2016: 14th European Conference, Amsterdam, The Netherlands, October 11–14, 2016, Proceedings, Part V 14*, pages 382–398. Springer, 2016. 7
- [2] Peter Anderson, Xiaodong He, Chris Buehler, Damien Teney, Mark Johnson, Stephen Gould, and Lei Zhang. Bottom-up and top-down attention for image captioning and visual question answering. In *Proceedings of the IEEE/CVF Conference on Computer Vision and Pattern Recognition*, pages 6077–6086, 2018. 3
- [3] Gautham Anil, Vishnu Vinod, and Apurva Narayan. Generating universal adversarial perturbations for quantum classifiers. In *Proceedings of the AAAI Conference on Artificial Intelligence*, pages 10891–10899, 2024. 3, 4
- [4] Shuang Bai and Shan An. A survey on automatic image caption generation. *Neurocomputing*, 311:291–304, 2018. 3
- [5] Satanjeev Banerjee and Alon Lavie. Meteor: An automatic metric for mt evaluation with improved correlation with human judgments. In *Proceedings of the acl workshop on intrinsic and extrinsic evaluation measures for machine translation and/or summarization*, pages 65–72, 2005. 7
- [6] Melika Behjati, Seyed-Mohsen Moosavi-Dezfooli, Mahdieh Soleymani Baghshah, and Pascal Frossard. Universal adversarial attacks on text classifiers. In *ICASSP 2019-2019 IEEE International Conference on Acoustics, Speech and Signal Processing (ICASSP)*, pages 7345–7349. IEEE, 2019. 6
- [7] Nicholas Carlini and David Wagner. Towards evaluating the robustness of neural networks. In *2017 IEEE Symposium on Security and Privacy (SP)*, pages 39–57. Ieee, 2017. 1
- [8] Fei-Long Chen, Du-Zhen Zhang, Ming-Lun Han, Xiu-Yi Chen, Jing Shi, Shuang Xu, and Bo Xu. Vlp: A survey on vision-language pre-training. *Machine Intelligence Research*, 20(1):38–56, 2023. 2
- [9] Yen-Chun Chen, Linjie Li, Licheng Yu, Ahmed El Kholy, Faisal Ahmed, Zhe Gan, Yu Cheng, and Jingjing Liu. Uniter: Universal image-text representation learning. In *Proceedings of the European Conference on Computer Vision (ECCV)*, pages 104–120. Springer, 2020. 2, 3
- [10] Gavin Weiguang Ding, Luyu Wang, and Xiaomeng Jin. Advtorch v0. 1: An adversarial robustness toolbox based on pytorch. *arXiv preprint arXiv:1902.07623*, 2019. 13
- [11] Virginie Do, Oana-Maria Camburu, Zeynep Akata, and Thomas Lukasiewicz. e-snli-ve: Corrected visual-textual entailment with natural language explanations. *arXiv preprint arXiv:2004.03744*, 2020. 12
- [12] Yinpeng Dong, Fangzhou Liao, Tianyu Pang, Hang Su, Jun Zhu, Xiaolin Hu, and Jianguo Li. Boosting adversarial attacks with momentum. In *Proceedings of the IEEE/CVF Conference on Computer Vision and Pattern Recognition*, pages 9185–9193, 2018. 15
- [13] Yifan Du, Zikang Liu, Junyi Li, and Wayne Xin Zhao. A survey of vision-language pre-trained models. *arXiv preprint arXiv:2202.10936*, 2022. 2
- [14] Gintare Karolina Dziugaite, Zoubin Ghahramani, and Daniel M Roy. A study of the effect of jpg compression on adversarial images. *arXiv preprint arXiv:1608.00853*, 2016. 13
- [15] Kevin Eykholt, Ivan Evtimov, Earlene Fernandes, Bo Li, Amir Rahmati, Chaowei Xiao, Atul Prakash, Tadayoshi Kohno, and Dawn Song. Robust physical-world attacks on deep learning visual classification. In *Proceedings of the IEEE/CVF Conference on Computer Vision and Pattern Recognition*, pages 1625–1634, 2018. 1
- [16] Weiwei Feng, Nanqing Xu, Tianzhu Zhang, and Yongdong Zhang. Dynamic generative targeted attacks with pattern injection. In *Proceedings of the IEEE/CVF Conference on Computer Vision and Pattern Recognition*, pages 16404–16414, 2023. 2
- [17] Haoran Gao, Hua Zhang, Jiahui Wang, Xin Zhang, Huawei Wang, Wenmin Li, and Tengfei Tu. Nuat-gan: Generating black-box natural universal adversarial triggers for text classifiers using generative adversarial networks. *IEEE Transactions on Information Forensics and Security*, 2024. 2, 3, 4
- [18] Jamie Hayes and George Danezis. Learning universal adversarial perturbations with generative models. In *2018 IEEE Security and Privacy Workshops (SPW)*, pages 43–49. IEEE, 2018. 3
- [19] Kaiming He, Haoqi Fan, Yuxin Wu, Saining Xie, and Ross Girshick. Momentum contrast for unsupervised visual representation learning. In *Proceedings of the IEEE/CVF Conference on Computer Vision and Pattern Recognition*, pages 9729–9738, 2020. 5
- [20] Richang Hong, Daqing Liu, Xiaoyu Mo, Xiangnan He, and Hanwang Zhang. Learning to compose and reason with language tree structures for visual grounding. *IEEE transactions on pattern analysis and machine intelligence*, 44(2): 684–696, 2019. 3
- [21] Andrej Karpathy and Li Fei-Fei. Deep visual-semantic alignments for generating image descriptions. In *Proceedings of the IEEE/CVF Conference on Computer Vision and Pattern Recognition*, pages 3128–3137, 2015. 6
- [22] Taewan Kim and Joydeep Ghosh. On single source robustness in deep fusion models. *Advances in Neural Information Processing Systems*, 32, 2019. 3
- [23] Junnan Li, Ramprasaath Selvaraju, Akhilesh Gotmare, Shafiq Joty, Caiming Xiong, and Steven Chu Hong Hoi. Align before fuse: Vision and language representation learning with momentum distillation. *Advances in Neural Information Processing Systems*, 34:9694–9705, 2021. 2, 3, 6, 7

- [24] Junnan Li, Dongxu Li, Caiming Xiong, and Steven Hoi. Blip: Bootstrapping language-image pre-training for unified vision-language understanding and generation. In *International conference on machine learning*, pages 12888–12900. PMLR, 2022. 2, 3, 6
- [25] Liunian Harold Li, Mark Yatskar, Da Yin, Cho-Jui Hsieh, and Kai-Wei Chang. Visualbert: A simple and performant baseline for vision and language. *arXiv preprint arXiv:1908.03557*, 2019. 2
- [26] Chin-Yew Lin. Rouge: A package for automatic evaluation of summaries. In *Text summarization branches out*, pages 74–81, 2004. 7
- [27] Tsung-Yi Lin, Michael Maire, Serge Belongie, James Hays, Pietro Perona, Deva Ramanan, Piotr Dollár, and C Lawrence Zitnick. Microsoft coco: Common objects in context. In *Computer Vision–ECCV 2014: 13th European Conference, Zurich, Switzerland, September 6–12, 2014, Proceedings, Part V 13*, pages 740–755. Springer, 2014. 6
- [28] Xuannan Liu, Yaoyao Zhong, Yuhang Zhang, Lixiong Qin, and Weihong Deng. Enhancing generalization of universal adversarial perturbation through gradient aggregation. In *Proceedings of the IEEE/CVF International Conference on Computer Vision*, pages 4435–4444, 2023. 3
- [29] Dong Lu, Zhiqiang Wang, Teng Wang, Weili Guan, Hongchang Gao, and Feng Zheng. Set-level guidance attack: Boosting adversarial transferability of vision-language pre-training models. In *Proceedings of the IEEE/CVF International Conference on Computer Vision*, pages 102–111, 2023. 2, 3, 5, 6, 7, 12, 15, 16
- [30] Seyed-Mohsen Moosavi-Dezfooli, Alhussein Fawzi, and Pascal Frossard. Deepfool: a simple and accurate method to fool deep neural networks. In *Proceedings of the IEEE/CVF Conference on Computer Vision and Pattern Recognition*, pages 2574–2582, 2016. 2
- [31] Seyed-Mohsen Moosavi-Dezfooli, Alhussein Fawzi, Omar Fawzi, and Pascal Frossard. Universal adversarial perturbations. In *Proceedings of the IEEE/CVF Conference on Computer Vision and Pattern Recognition*, pages 1765–1773, 2017. 2, 3
- [32] Konda Reddy Mopuri, Aditya Ganeshan, and R Venkatesh Babu. Generalizable data-free objective for crafting universal adversarial perturbations. *IEEE transactions on pattern analysis and machine intelligence*, 41(10):2452–2465, 2018. 3
- [33] Muzammal Naseer, Salman Khan, Munawar Hayat, Fahad Shahbaz Khan, and Fatih Porikli. A self-supervised approach for adversarial robustness. In *Proceedings of the IEEE/CVF Conference on Computer Vision and Pattern Recognition*, pages 262–271, 2020. 13
- [34] Weili Nie, Brandon Guo, Yujia Huang, Chaowei Xiao, Arash Vahdat, and Anima Anandkumar. Diffusion models for adversarial purification. *arXiv preprint arXiv:2205.07460*, 2022. 13, 15
- [35] Kishore Papineni, Salim Roukos, Todd Ward, and Wei-Jing Zhu. Bleu: a method for automatic evaluation of machine translation. In *Proceedings of the 40th annual meeting of the Association for Computational Linguistics*, pages 311–318, 2002. 7
- [36] Bryan A Plummer, Liwei Wang, Chris M Cervantes, Juan C Caicedo, Julia Hockenmaier, and Svetlana Lazebnik. Flickr30k entities: Collecting region-to-phrase correspondences for richer image-to-sentence models. In *Proceedings of the IEEE international conference on computer vision*, pages 2641–2649, 2015. 6
- [37] Omid Poursaeed, Isay Katsman, Bicheng Gao, and Serge Belongie. Generative adversarial perturbations. In *Proceedings of the IEEE/CVF Conference on Computer Vision and Pattern Recognition*, pages 4422–4431, 2018. 2, 6
- [38] Alec Radford, Jong Wook Kim, Chris Hallacy, Aditya Ramesh, Gabriel Goh, Sandhini Agarwal, Girish Sastry, Amanda Askell, Pamela Mishkin, Jack Clark, et al. Learning transferable visual models from natural language supervision. In *International conference on machine learning*, pages 8748–8763. PMLR, 2021. 3, 6
- [39] Ramakrishna Vedantam, C Lawrence Zitnick, and Devi Parikh. Cider: Consensus-based image description evaluation. In *Proceedings of the IEEE/CVF Conference on Computer Vision and Pattern Recognition*, pages 4566–4575, 2015. 7
- [40] Donghua Wang, Wen Yao, Tingsong Jiang, and Xiaoqian Chen. Improving transferability of universal adversarial perturbation with feature disruption. *IEEE Transactions on Image Processing*, 2023. 3
- [41] Haodi Wang, Kai Dong, Zhilei Zhu, Haotong Qin, Aishan Liu, Xiaolin Fang, Jiakai Wang, and Xianglong Liu. Transferable multimodal attack on vision-language pre-training models. In *2024 IEEE Symposium on Security and Privacy (SP)*, pages 102–102. IEEE Computer Society, 2024. 2, 3, 5, 6, 12, 13, 15
- [42] Kaiye Wang, Qiyue Yin, Wei Wang, Shu Wu, and Liang Wang. A comprehensive survey on cross-modal retrieval. *arXiv preprint arXiv:1607.06215*, 2016. 3
- [43] Ning Xie, Farley Lai, Derek Doran, and Asim Kadav. Visual entailment: A novel task for fine-grained image understanding. *arXiv preprint arXiv:1901.06706*, 2019. 3, 6, 12
- [44] Jinyu Yang, Jiali Duan, Son Tran, Yi Xu, Sampath Chanda, Liqun Chen, Belinda Zeng, Trishul Chilimbi, and Junzhou Huang. Vision-language pre-training with triple contrastive learning. In *Proceedings of the IEEE/CVF Conference on Computer Vision and Pattern Recognition*, pages 15671–15680, 2022. 6
- [45] Karren Yang, Wan-Yi Lin, Manash Barman, Filipe Condessa, and Zico Kolter. Defending multimodal fusion models against single-source adversaries. In *Proceedings of the IEEE/CVF Conference on Computer Vision and Pattern Recognition*, pages 3340–3349, 2021. 3
- [46] Licheng Yu, Patrick Poirson, Shan Yang, Alexander C Berg, and Tamara L Berg. Modeling context in referring expressions. In *Computer Vision–ECCV 2016: 14th European Conference, Amsterdam, The Netherlands, October 11–14, 2016, Proceedings, Part II 14*, pages 69–85. Springer, 2016. 6
- [47] Yan Zeng, Xinsong Zhang, and Hang Li. Multi-grained vision language pre-training: Aligning texts with visual concepts. In *International conference on machine learning*, pages 25994–26009. PMLR, 2022. 6

- [48] Jiaming Zhang, Qi Yi, and Jitao Sang. Towards adversarial attack on vision-language pre-training models. In *Proceedings of the 30th ACM International Conference on Multimedia*, pages 5005–5013, 2022. [1](#), [2](#), [3](#), [5](#), [6](#), [12](#), [15](#), [16](#)
- [49] Peng-Fei Zhang, Zi Huang, and Guangdong Bai. Universal adversarial perturbations for vision-language pre-trained models. In *Proceedings of the 47th International ACM SIGIR Conference on Research and Development in Information Retrieval*, pages 862–871, 2024. [2](#), [3](#), [6](#)
- [50] Tianyi Zhang, Varsha Kishore, Felix Wu, Kilian Q Weinberger, and Yoav Artzi. Bertscore: Evaluating text generation with bert. In *International Conference on Learning Representations*. [15](#)
- [51] Ziqi Zhou, Shengshan Hu, Ruizhi Zhao, Qian Wang, Leo Yu Zhang, Junhui Hou, and Hai Jin. Downstream-agnostic adversarial examples. In *Proceedings of the IEEE/CVF International Conference on Computer Vision*, pages 4345–4355, 2023. [3](#)

A. Pseudocode of the Proposed Algorithm

We present the pseudocode of our proposed attack algorithm for image modality in Alg. 1. Note that the text attacks are completely symmetrical as illustrated in Sec. 3.

Algorithm 1 Pseudocode of universal image attacks

Require: $G_w(\cdot)$: the perturbation generator; D_s : the multimodal training set; f_I, f_T : image encoder and text encoder of the surrogate VLP model; K : the max iteration; ϵ_v : the perturbation budget; N : the scaling times;

Ensure: Universal image perturbation δ_v ;

- 1: **Initialize** the fixed noise z_v with Gaussian distribution;
- 2: **for** $i \leftarrow 0$ to K **do**
- 3: Randomly sample an image-text pair $(v, \mathbf{t}) \sim D_s$;
- 4: $\delta_v = \text{Clip}_{\epsilon_v}(G_w(z_v; f_T(\mathbf{t}))), v_{adv} = v + \delta_v$;
- 5: Augment v and v_{adv} into different scales and apply random Gaussian noises to obtain $\mathbf{v} = \{v_1 \dots, v_N\}$ and $\mathbf{v}_{adv} = \{v_1^{adv} \dots, v_N^{adv}\}$;
- 6: Randomly sample a batch of text sets from D_s and obtain $\mathbf{t}_{pos} = \{t'_1 \dots, t'_K\}$ by selecting the one with the farthest feature distance from the clean image v ;
- 7: Compute \mathcal{L}_{CL} with $\mathbf{v}_{adv}, \mathbf{t}$ and \mathbf{t}_{pos} by Eq. (3);
- 8: Compute \mathcal{L}_{Dis} with \mathbf{v} and \mathbf{v}_{adv} by Eq. (4);
- 9: Optimize the generator G_w based on Eq. (5);
- 10: Backward pass and update G_w ;
- 11: **end for**
- 12: **Return** δ_v

B. More Training Details

For Flickr30K and MSCOCO, we randomly sample 30,000 images and their captions from the training set to train our perturbation generator. For SNLI-VE and RefCOCO+, we learn the C-PGC directly using their training set with 29,783 and 16,992 images respectively. Since an image corresponds to multiple text descriptions in these datasets, we calculate the average of their textual embedding as the multimodal condition for the cross-attention modules.

We initialize the noise variable z_v as a 3×3 matrix. Meanwhile, the initial noise z_t 's dimensions in the text modality depend on the size of the hidden layer within the specific VLP model. Concretely, we set its dimension to 1×3 for ALBEF, TCL, BLIP, and X-VLM, while 1×2 for the CLIP model. When computing the multimodal contrastive loss \mathcal{L}_{CL} , the temperature τ is set as 0.1. The generator is trained over 40 epochs with the Adam optimizer at a learning rate of 2^{-4} . Following previous works [29, 41], we employ the attack success rate (ASR) as our quantitative measurement in ITR tasks by computing the extent to which the adversarial perturbations result in victim models' performance deviations from the clean performance.

C. More Experimental Results

In this section, we provide more experimental results of our method in various tasks and scenarios.

Visual entailment tasks. Given an image and a textual description, visual entailment involves determining whether the textual description can be inferred from the semantic information of the image. We align with previous VLP attacks [41, 48] and conduct experiments on the SNLI-VE [43] dataset using the ALBEF and TCL models. Note that the Baseline represents the clean performance of the target model on the clean data and the orange and green indicate ALBEF and TCL as source models respectively. The results presented in Fig. 6 reveal that C-PGC obtains impressive attack effects by decreasing the average accuracy by nearly 20%.

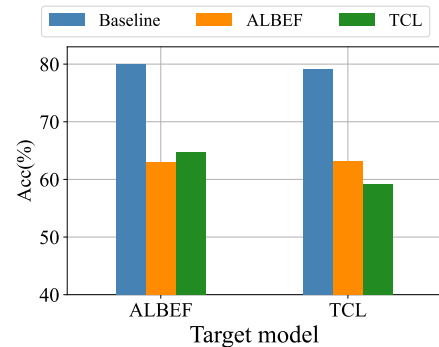


Fig. 6: Accuracy of VE tasks for different source and target models. The Baseline indicates the clean performance.

Notably, [11] has reported a large number of annotation errors in the labels of the SNLI-VE corpus used for VE tasks. Therefore, the presented results are only for experimental integrity and reference purposes.

Image-text retrievals on MSCOCO dataset. We then supplement the ASR of the ITR tasks on the MSCOCO dataset in Table 5. The results again reveal that C-PGC greatly enhances the attack. Particularly in the more realistic and challenging transferable scenarios, the proposed method achieves considerably better performance, e.g., 82.49% and 76.24% increase in ASR of TR and IR tasks when transferring from ALBEF to TCL, confirming the superiority of our contrastive learning-based paradigm.

Cross-domain scenarios. We proceed to discuss the attack performance of the proposed algorithm in a more challenging scenario where there is an obvious distribution shift between the training dataset and the test samples. Specifically, we generate universal adversarial perturbations based on MSCOCO or Flickr30K and evaluate them accordingly on the other dataset. We present the attack success rates on the retrieval tasks across six models in Table 6. It can be observed that the domain gap indeed has a negative effect

Table 5. ASR (%) of different methods for image-text retrieval tasks on MSCOCO dataset. TR indicates text retrieval based on the input image, while IR is image retrieval using the input text.

Source	Method	ALBEF		TCL		X-VLM		CLIP _{vIT}		CLIP _{CNN}		BLIP	
		TR	IR	TR	IR	TR	IR	TR	IR	TR	IR	TR	IR
ALBEF	GAP	82.65	84.35	53.6	45.46	15.09	15.64	25.18	29.94	28.06	35.28	37.44	33.61
	ETU	83.6	88.98	27.43	24.47	20.39	19.94	28.54	35.05	37.01	44.72	22.25	22.03
	Ours	96.18	95.09	82.49	76.24	39.97	48.58	59.71	67.05	61.27	70.8	59.18	63.89
TCL	GAP	55.92	48.22	95.16	92.29	17.34	17.01	28.73	31.19	32.27	39.81	43.59	39.64
	ETU	60.09	50.62	93.28	89.28	27.19	25.41	33	37.86	45.83	52.24	39.59	36.31
	Ours	76.62	71.17	96.72	93.88	42.99	48.4	70.32	79.08	74.1	82.97	62.35	66.97
X-VLM	GAP	26.35	23.72	27.8	22.91	95.1	88.84	32.39	38.16	52	55.4	24.67	22.65
	ETU	22.94	21.63	22.01	19.65	96.23	92.97	28.81	34.26	48.53	52.74	20.52	19.3
	Ours	51.46	65.71	52.8	64.99	98.89	95.79	67.42	75.45	75.49	82.58	55.74	66.7
CLIP _{vIT}	GAP	35.96	31.91	37.33	32.56	33.42	29.25	97.71	96.04	74.63	74.67	33.47	31.99
	ETU	31.5	29.62	33.25	30.38	32.36	29.92	95.88	96.34	82.07	83.41	30.62	30.7
	Ours	46.92	53.89	46.03	50.87	41.49	48.6	98.74	98.01	81.58	86.5	47.35	57.55
CLIP _{CNN}	GAP	13.57	25.21	19.05	28.87	11.59	23.13	27.46	43.16	73.18	81.6	15.25	27.94
	ETU	21.71	21.92	22.33	22.8	24.77	23.93	34.99	40.3	95.34	95.14	20.06	22.26
	Ours	33.41	47.96	38.81	50.78	36.59	48.83	66.04	72.59	94.73	95.21	42.39	57.84
BLIP	GAP	12.23	23.94	14.49	25.44	6.91	17.81	20.32	37.00	26.81	43.59	47.21	73.33
	ETU	46.07	43.27	44.58	37.61	33.14	29.85	33.77	40.02	48.28	52.88	81.27	83.59
	Ours	61.95	60.92	60.95	59.57	51.81	52.53	62.23	72.51	69.61	78.44	91.67	90.42

Table 6. ASR (%) of Cross-domain attacks on six models from Flickr30k to MSCOCO and vice versa.

Setting	Source	ALBEF		TCL		X-VLM		CLIP _{vIT}		CLIP _{CNN}		BLIP	
		TR	IR	TR	IR	TR	IR	TR	IR	TR	IR	TR	IR
Flickr30K ↓ MSCOCO	ALBEF	96.83	94.69	81.46	74.87	44.79	51.64	63.68	73.06	69.77	78.09	68.88	70.61
	TCL	78.27	73.17	97.83	95.03	40.46	47.34	64.98	73.27	70.96	78.18	63.71	67.1
	X-VLM	50.63	65.91	53.23	65.65	95.91	93.32	65.51	74.72	75.69	81.93	57.69	67.28
	CLIP _{vIT}	49.88	53.39	49.47	52.21	47.77	48.52	95.5	97.01	83.05	85.38	50.97	57.93
	CLIP _{CNN}	43.05	54.19	43.04	54.39	43.73	53.94	67.3	74.39	98.61	97.41	47.22	59.11
	BLIP	54.45	55.51	55.63	53.02	41.07	46.93	61.69	69.24	65.52	75.23	83.19	82.17
MSCOCO ↓ Flickr30K	ALBEF	88.08	87.28	58.9	61.53	17.58	36.07	39.78	61.08	47.28	64.95	35.02	49.4
	TCL	47.58	53.7	87.27	83.55	18.6	34.45	51.85	72.22	59.46	76.09	37.75	53.08
	X-VLM	25.39	46.74	27.33	49.13	79.98	81.72	42.73	66.48	59.46	73.07	31.65	51.48
	CLIP _{vIT}	21.07	39.47	24.53	42.44	15.45	36.52	93.97	95.53	62.95	77.21	25.55	45.91
	CLIP _{CNN}	13.87	37.93	19.36	41.25	15.85	37.47	42.61	66.73	85.75	88.76	22.92	48.45
	BLIP	33.2	46.07	36.02	47.97	23.58	38.48	43.97	65.3	56.35	71.08	71.91	73.62

on attack performance. However, our method still maintains excellent ASR in most cases, unveiling its outstanding cross-domain transferability.

Results of R@5 and R@10. As aforementioned, we supplement the ASR of the ITR tasks based on R@5 and R@10 metrics and provide the attack success rates in Table 7. Obviously, our proposed C-PGC still consistently attains better performance than the baseline method ETU, regardless of the evaluation measurements for retrieval results.

Performance under Defenses. We next analyze several

defense strategies to mitigate the potential harm from C-PGC. Concretely, we totally align with TMM [41] and consider several input preprocessing-based schemes, including image smoothing [10] (Gaussian, medium, average smoothing), JPEG compression [14], NRP [33], and the DiffPure [34], a powerful purification defense using diffusion models. For adversarial text correction, we choose the LanguageTool (LT) [41], which has been widely adopted in various scenarios due to its universality and effectiveness.

The attack results in Table 8 demonstrate that the pro-

Table 7. Attack success rates (%) regarding R@5 and R@10 metrics of our C-PGC and ETU for image-text retrieval tasks.

Dataset	Source	Method	ALBEF		TCL		X-VLM		CLIP _{VIT}		CLIP _{CNN}		BLIP	
			TR	IR	TR	IR	TR	IR	TR	IR	TR	IR	TR	IR
Flickr30K (R@5)	ALBEF	ETU	68.54	77.68	14.41	14.43	4.1	6.41	6.11	16.97	11.57	23.11	9.36	13.3
		Ours	83.67	80.02	41.84	42.18	6.9	17.19	18.34	41.03	26.22	49.42	24.25	34.59
	TCL	ETU	14.43	16.23	84.88	80.43	2.4	5.8	5.6	17.37	13.27	24.27	7.24	10.98
		Ours	29.76	35.62	90.89	84.18	3.2	13.65	20.93	42.06	25.27	49.1	16.5	30.32
	X-VLM	ETU	3.81	5.85	3.9	6.51	89.2	84.57	5.18	16.9	14.33	24.52	3.12	7.81
		Ours	7.62	25.1	8.71	26.63	89.2	85.84	19.38	42.48	30.89	50.7	13.68	29
CLIP _{VIT}	ETU	5.31	7.88	7.51	10.42	4.7	8.92	76.42	84.54	35.46	41.73	5.03	10.2	
	Ours	6.31	17.51	8.01	19.65	4.3	15.1	76.89	85.2	39.6	54.68	9.15	23.23	
CLIP _{CNN}	ETU	1.7	5.02	3.4	7.16	1.4	6.02	6.22	17.61	84.39	87.85	2.31	8.26	
	Ours	4.41	19.8	6.41	25.19	4.8	23.49	18.76	43.82	90.34	88.12	8.95	26.89	
BLIP	ETU	8.22	10.11	6.71	10.46	3.2	5.62	5.28	16.39	9.24	21.97	45.98	73.75	
	Ours	14.43	21.67	13.91	21.59	5.4	14.54	18.03	36.26	23.89	44.79	59.26	74.82	
MSCOCO (R@5)	ALBEF	ETU	81.73	88.76	13.45	11.51	9.01	9.32	16.85	20.74	22.6	28.86	10.96	12.02
		Ours	93.36	91.56	70.76	62.31	19.97	30.46	41.58	51.23	44.14	55.98	41.08	49.22
	TCL	ETU	44.94	36.45	90.21	84.54	13.46	13.1	19.52	23.03	30.81	36.37	25.63	25.11
		Ours	60.62	56.21	94.89	90.33	22.08	30.38	53.14	64.98	58.85	70.77	45.28	53.55
	X-VLM	ETU	11.03	11.11	10.22	9.24	94.36	90.02	17.56	20.8	33.45	38.14	10.08	10.12
		Ours	31.59	48.69	32.1	48.11	96.7	91.66	49.53	60.82	59.83	69.59	37.4	52.5
CLIP _{VIT}	ETU	15.89	16.01	18.61	16.11	16.45	16.61	93.12	94.66	72.97	75.5	17.1	19.26	
	Ours	25.69	35.95	24.69	33.14	21.37	31.38	96.7	96.49	70.76	77.86	28.72	42.01	
CLIP _{CNN}	ETU	9.55	10.34	9.9	10.95	10.98	11.96	22.63	26.84	90.7	92.07	9.69	12.25	
	Ours	16.83	31	19.86	34.54	18.84	34.02	50.21	59.2	90.94	90.43	25.5	44.89	
BLIP	ETU	29.6	29.6	26.95	21.97	17.67	16.14	20.83	24.27	32.77	36.72	76.16	80.69	
	Ours	42.56	43.73	41.72	41.8	31.05	35.63	44.37	57.9	54.47	66.01	81.71	81.91	
Flickr30K (R@10)	ALBEF	ETU	65.8	74.89	10	9.36	2.8	3.79	2.43	11.04	6.95	15.79	6.62	8.57
		Ours	80.5	75.17	34.8	34.28	4.2	11.72	9.83	31.14	16.87	39.40	18.76	27.08
	TCL	ETU	11.4	11.35	82.2	77.33	1.6	3.38	3.04	10.63	7.06	17.14	4.91	7.34
		Ours	24.2	27.32	89.2	80.73	2.1	9.33	12.77	32.4	16.97	38.63	12.54	24.1
	X-VLM	ETU	1.9	3.48	2.4	3.48	87.1	81.87	3.14	10.91	8.59	16.66	2.01	4.72
		Ours	4.1	17.79	4.6	19.27	86.3	82.94	11.14	31.49	21.06	40.3	7.32	21.81
CLIP _{VIT}	ETU	3.6	4.75	4.6	6.43	2.7	5.47	68.17	78.93	27.2	32.94	3.11	6.35	
	Ours	4.2	11.45	4.6	13.08	2.8	10.15	67.98	79.46	29.75	45.56	5.52	17.23	
CLIP _{CNN}	ETU	0.6	2.64	1.6	3.86	0.7	3.48	3.65	11.32	80.37	85.18	1.2	5.31	
	Ours	2.4	14.59	3.5	18.36	2.3	17.95	11.75	34.23	86.4	83.83	5.52	20.86	
BLIP	ETU	6.5	6.52	4.9	6.57	1.8	3.32	2.63	10.52	5.52	14.57	42.43	71.26	
	Ours	11.2	15.49	9.1	14.14	2.8	10.19	9.83	27.46	14.83	34.43	53.46	72	
MSCOCO (R@10)	ALBEF	ETU	81.14	87.58	9.08	7.92	5.44	6.33	12.62	16.15	17.71	23.05	7.63	9.15
		Ours	91.58	89.62	64.5	55.3	13.81	23.34	33.3	43.75	35.82	48.38	33.77	43.11
	TCL	ETU	38.6	30.39	88.56	82.6	8.92	9.3	14.61	18.43	25.24	30.06	20.37	21.41
		Ours	52.59	49.09	93.63	88.53	15.04	23.25	44.22	58.02	50.16	63.95	37.77	47.26
	X-VLM	ETU	7.41	7.37	6.76	6.27	93.17	88.66	12.93	16.43	28.32	32.47	6.73	8.01
		Ours	23.01	40.39	23.15	40.07	94.97	88.95	40.24	53.74	52	62.7	30.43	45.67
CLIP _{VIT}	ETU	11.05	11.5	13.67	11.67	11.21	12.14	91.47	93.8	67.7	71.14	13.03	15.4	
	Ours	17.87	28.52	17.48	26.09	14	24.67	95.55	95.31	64.04	72.75	22.05	35.65	
CLIP _{CNN}	ETU	6.05	7.02	6.54	7.54	6.97	8.36	17.65	21.66	88.13	90.16	6.73	9.45	
	Ours	10.77	24.11	13.34	27.53	12.31	28.03	41.33	52.02	88.28	87.14	20.26	39.43	
BLIP	ETU	23.63	24.4	19.69	16.37	11.55	11.86	16.3	19.66	26.04	30.64	73.88	77.63	
	Ours	33.64	36.14	32.15	33.8	22.64	28.52	36.07	50.3	47	59.07	78.39	78.98	

Table 8. ASR (%) of ITR tasks under defense strategies. The surrogate model is ALBEF and the dataset is Flickr30K. LT denotes the LanguageTool that corrects adversarial words within the sentence.

Method	ALBEF		TCL		X-VLM		CLIP _{VIT}		CLIP _{CNN}		BLIP	
	TR	IR	TR	IR	TR	IR	TR	IR	TR	IR	TR	IR
Gaussian	37.92	49.49	32.4	47.04	19.31	37.79	42.49	65.61	50	72.23	29.65	48.77
Medium	53.13	61.6	39.54	51.96	20.43	39.69	46.31	66.92	57.9	74.51	33.75	52.68
Average	29.09	44.91	29.61	44.72	17.89	36.07	42.98	65.42	49.74	72.48	27.55	46.9
JPEG	59.3	63.7	42.34	52.52	21.65	41.58	41.26	65.77	53.5	72.62	37.01	55.04
DiffPure	64.34	74.63	65.22	74.8	66.06	75.19	78.08	86.7	82.25	88.03	70.45	79.09
NRP	32.33	40.63	20.19	39.23	14.63	32.62	48.4	69	59.72	74.09	30.28	52.2
NRP+LT	29.05	35.23	21.33	37.41	15.55	29.63	47.19	67.35	56.82	73.47	28.23	50.59

Table 9. ASR results of the proposed method with different loss functions on Flickr30 when the surrogate model is ALBEF.

Method	ALBEF		TCL		X-VLM		CLIP _{VIT}		CLIP _{CNN}		BLIP	
	TR	IR	TR	IR	TR	IR	TR	IR	TR	IR	TR	IR
\mathcal{L}_{MSE}	12.02	30.75	14.39	35.08	11.41	30.79	37.32	56.05	40.17	56.39	19.66	37.33
\mathcal{L}_{Cos}	57.55	67.4	37.06	49.45	10.7	28.48	37.49	58.3	40.87	58.39	23.33	39.44
\mathcal{L}_{CL}	76.46	82.46	56.52	62.61	14.33	33.61	42.98	62.81	46.11	65.58	27.13	46.44
$\mathcal{L}_{MSE}+\mathcal{L}_{Dis}$	81.09	83.71	48.76	56.54	17.58	35.72	41.5	64.72	47.41	70.34	35.96	51.76
$\mathcal{L}_{Cos}+\mathcal{L}_{Dis}$	65.20	72.71	36.13	50.06	18.63	36.74	42.23	65.17	50.91	69.78	36.91	50.69
$\mathcal{L}_{CL}+\mathcal{L}_{Dis}$	90.13	88.82	62.11	64.48	20.53	39.38	43.1	65.93	54.4	72.51	44.79	56.36

posed attack still attains great ASR against different powerful defenses. It also indicates that NRP+LT would be a decent choice to alleviate the threat brought by C-PGC. Another noteworthy finding is that, although DiffPure [34] exhibits remarkable performance in defending attacks in classification tasks, its ability is greatly reduced in V+L scenarios since the denoising process could also diminish some texture or semantic information that is critical for VLP models, thereby acquiring unsatisfactory defense effects.

D. Rationality behind the Loss Design

It is widely acknowledged that contrastive learning serves as a powerful and foundational tool for modality alignment in VLP models, establishing a nearly point-to-point relationship between image and text features. Since contrastive learning can establish robust and precise alignment, leveraging the same technique to disrupt the established alignment is also promising to yield effective performance.

Taking image attack as an example, the underlying principle behind our contrastive learning-based attack can be understood from two perspectives:

- Leverage the originally matched texts as negative samples to push aligned image-text pairs apart. This broadly corresponds to the objective of traditional untargeted adversarial attacks.
- Additionally, the proposed paradigm introduces dissimilar texts as positive samples to further pull the adversarial

image out of its original subspace and relocate it to an incorrect feature area.

By simultaneously harnessing the collaborative effects of *push* (negative samples) and *pull* (positive samples), the proposed contrastive framework achieves exceptional attack performance, which has been validated by comprehensive experimental results. Besides, we also explore several potential alternative loss functions that more directly align with the common goal of untargeted attack in Table 9, including maximizing the cosine distance \mathcal{L}_{Cos} or MSE distance \mathcal{L}_{MSE} between features of matched image-text pairs.

Recall that \mathcal{L}_{CL} and \mathcal{L}_{Dis} denote our designed contrastive loss and unimodal loss terms respectively. As observed, the integration of \mathcal{L}_{CL} consistently brings significant ASR improvements, verifying the rationality and superiority of the adopted contrastive loss.

E. Semantic Similarity Analysis

The basic objective of untargeted adversarial attacks is to fool the victim model to output incorrect predictions [12], while the attacker is supposed to preserve semantic similarity between original and adversarial samples to ensure attack imperceptibility. In our implementation, we follow the rigorous setup in prior works [29, 41, 48] that modify only one single word to preserve the attack stealthiness. To quantitatively analyze the influence, we provide the BERT scores [50], which calculate the P (precision), R (recall), and F1

Table 10. Comparison of BERTScore between clean and adversarial texts across different surrogate models.

Method	ALBEF			TCL			CLIP _{VIT}			CLIP _{CNN}		
	P	R	F1	P	R	F1	P	R	F1	P	R	F1
Co-Attack [48]	0.8328	0.8589	0.8455	0.8325	0.8588	0.8453	0.8269	0.8526	0.8394	0.8271	0.8530	0.8397
SGA [29]	0.8389	0.8654	0.8518	0.8376	0.8646	0.8509	0.8416	0.8697	0.8553	0.8378	0.8650	0.8511
Ours	0.8891	0.8613	0.8748	0.8924	0.8687	0.8802	0.8746	0.8684	0.8713	0.8948	0.8842	0.8893

(F1 score), to measure the semantic distance between 5,000 clean and adversarial sentences in Table 10. Note that we provide existing well-acknowledged sample-specific algorithms Co-Attack [48] and SGA [29] as references.

As observed, C-PGC generally acquires higher similarity scores than existing sample-specific methods across various surrogate models, which validates that C-PGC achieves an eligible perturbation strategy in terms of text perturbation imperceptibility. Basically, the lower semantic similarity of sample-specific approaches stems from their word-selection mechanism, which maximizes the semantic distance tailored to every input sentence for attack enhancement. *I.e.*, these methods select the adversarial word that maximizes the distance between the original and perturbed texts for every input sentence, which inherently leads to relatively larger semantic deviations. This highlights that our method achieves a better balance between efficacy and stealthiness.

F. Multimodal Alignment Destruction

To provide more intuitive evidence that our C-PGC successfully destroys the image-text alignment relationship, we compute the distance between the encoded image and text embeddings before and after applying the UAP. For an input pair (v, t) , we calculate the relative distance d_{rel} by:

$$d_{rel} = \frac{\|f_I(v + \delta_v) - f_T(t \oplus \delta_t)\|_2 - \|f_I(v) - f_T(t)\|_2}{\|f_I(v) - f_T(t)\|_2} \quad (6)$$

We provide the distances averaged on 5000 image-text pairs from Flickr30K in Table 11. Benefiting from our delicate designs, C-PGC achieves better disruption of the aligned multimodal relationship, thereby boosting the generalization ability and transferability of the produced UAP.

Table 11. Average relative cross-modal feature distances.

Source	Method	ALBEF	TCL	BLIP	X-VLM	CLIP _{VIT}	CLIP _{CNN}
ALBEF	GAP	7.18	6.54	0.91	1.74	0.31	0.98
	ETU	8.70	8.02	0.81	2.85	0.36	1.32
	C-PGC	8.83	14.95	2.73	6.09	3.42	3.92
TCL	GAP	4.02	24.27	0.91	0.87	0.12	0.07
	ETU	5.57	26.32	0.55	2.56	1.47	0.55
	C-PGC	6.43	27.11	3.64	4.35	2.56	2.94
BLIP	GAP	3.17	4.67	11.82	1.74	-1.71	-0.98
	ETU	5.26	6.03	13.14	2.90	0.25	1.14
	C-PGC	6.41	12.15	13.64	4.35	1.71	1.96

G. Discussions and Future Directions

Overlook of interactions between perturbations δ_v and δ_t . The proposed framework generates universal perturbations for image and text respectively based on the designed loss functions. Despite the remarkable performance, it does not consider interactions between δ_v and δ_t during the optimization. Future research can explore this limitation as a potential mechanism to further strengthen the attack.

Textual Semantic consistency. To ensure the stealthiness of text attacks, we set the perturbation budget $\epsilon_t = 1$, *i.e.*, only one word is modified. Although C-PGC obtains superior semantic similarity to previous sample-specific methods, there is still room to improve from the proposed C-PGC. Moreover, future studies can consider similarity preservation strategies by applying more effective constraints during the generator training or adversarial sentences post-processing to facilitate a more stealthy attack.

H. More Visualization Results

This section presents a rich visual analysis of the proposed attack on a series of downstream tasks. Specifically, we first provide the visualization of the image retrieval task using the MSCOCO dataset in Fig. 7. Besides, we generate the UAP using the ALBEF model for the visual grounding (VG) task. As illustrated in Fig. 8, the prediction bounding boxes exhibit a notable deviation from the clean predictions, verifying that our generated adversarial samples significantly interfere with the multimodal alignment. In the visual entailment (VE) task, we employ BLIP as the victim model and present the results in Fig. 9. These qualitative visualizations again demonstrate the remarkable attack effects of our proposed method on various downstream tasks.

Mountain climber
luckily safely lands
in the water.



A person in blue is
the only person
luckily currently
throwing their ball
at a bowling alley.



ALBEF

TCL

X-VLM

CLIP_{VIT}

CLIP_{CNN}

BLIP

Fig. 7: Attacks results of C-PGC on the image retrieval task. The red indicates the UAP and the crossed-out word is the replaced one. We generate the word on ALBEF and test it on 6 target models. All retrieved images fail to correspond to the query text, validating the rationality of our contrastive learning-based attacks.

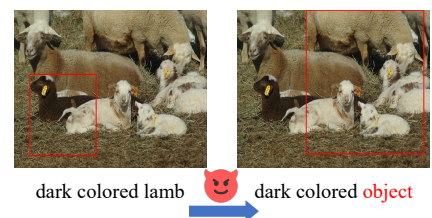
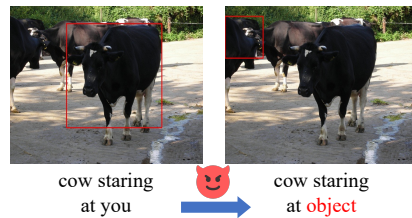
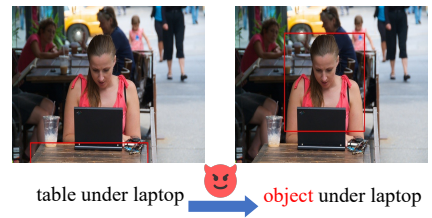
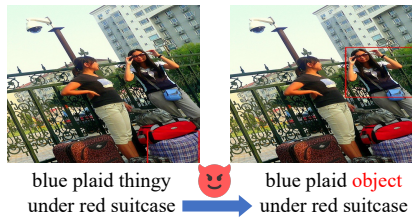
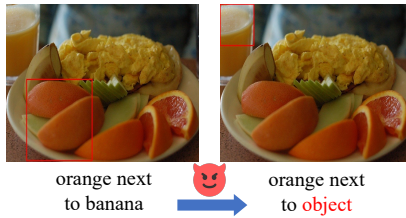
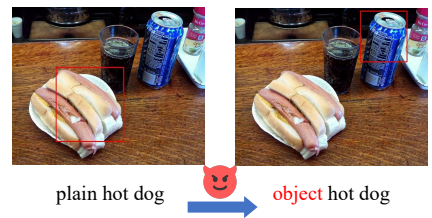
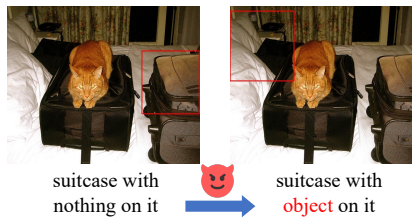
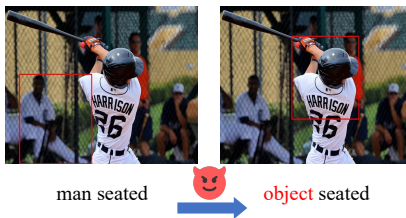
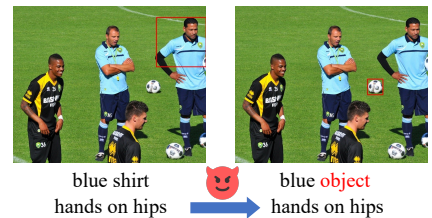
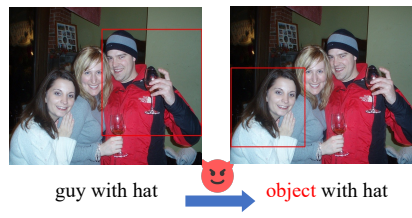
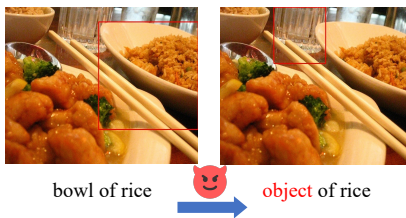


Fig. 8: Illustration of visual grounding. The predictions of clean pairs are on the left while the predictions of adversarial samples are on the right. The red word is the adversarial word perturbation.

			
The guys are walking in the park.	The guys are getting in the park.	Two surfers out surfing in the early morning.	Two surfers out getting in the early morning.
Neutral	Contradiction	Neutral	Contradiction
			
A superhero is riding a horse.	A superhero is getting a horse.	A semi-trailer is unloaded by a group of people.	A semi-trailer is getting by a group of people.
Neutral	Entailment	Neutral	Entailment
			
A dog is sprinting across the ground.	A dog is getting across the ground.	The men are cooking in the kitchen.	The men are getting in the kitchen.
Entailment	Contradiction	Entailment	Contradiction
			
A street vendor is selling toys.	A street vendor is getting toys.	A man holds a large bass drum.	A man getting a large bass drum.
Entailment	Neutral	Entailment	Neutral
			
The toddler gave their friend a red cape.	The toddler getting their friend a red cape.	A father and a son are playing baseball.	A father and a son are getting baseball.
Contradiction	Neutral	Contradiction	Neutral
			
The statue is on the water.	The statue is getting the water.	Five men are dressed as pumpkins.	Five men are getting as pumpkins.
Contradiction	Entailment	Contradiction	Entailment

Fig. 9: Illustration of the visual entailment task. The red indicates the universal adversarial word. It can be observed that all predictions do not match with the ground truth.